Advanced Composite Materials
Publication details, including instructions for authors and subscription information:
http://www.tandfonline.com/loi/tacm20

Experimental characterization of microscopic damage progress in AS4/PEEK cross-ply laminates under thermal cycling

Kazuhiro Terada , Satoshi Kobayashi & Nobuo Takeda
Version of record first published: 02 Apr 2012.

To cite this article: Kazuhiro Terada , Satoshi Kobayashi & Nobuo Takeda (2000): Experimental characterization of microscopic damage progress in AS4/PEEK cross-ply laminates under thermal cycling, Advanced Composite Materials, 9:4, 335-348

To link to this article: http://dx.doi.org/10.1163/15685510052000147

Adv. Composite Mater., Vol. 9, No. 4, pp. 335–348 (2000)

Experimental characterization of microscopic damage progress in AS4/PEEK cross-ply laminates under thermal cycling

KAZUHIRO TERADA [1,*], SATOSHI KOBAYASHI [1] and NOBUO TAKEDA [2]

[1] *Takeda Laboratory, Komaba Open Laboratory (KOL), The University of Tokyo, 4-6-1 Komaba, Meguro-ku, Tokyo 153-8904, Japan*

[2] *Graduate School of Frontier Sciences, The University of Tokyo, 7-3-1 Hongo, Bunkyo-ku, Tokyo 113-8656, Japan*

Received 9 March 2000; accepted 28 June 2000

Abstract—Microscopic damage progress in high temperature CFRP cross-ply laminates under thermal cycling was investigated. Two types of laminate configuration were tested to study the effect of ply thickness. Matrix cracks initiated in both 0° and 90° plies and the number of cracks increased as the number of cycles increased. The saturated number of cracks in 90° plies was twice as large as that in 0° plies. To discuss these experimental results, shear-lag analysis was used to evaluate both the energy release rate associated with matrix cracking and the thermal residual stress in cracked plies. It was implied that the effect of the maximum thermal residual stress as well as the energy release rate range were significant in the quantitative evaluation of the matrix cracking induced by the thermal cycling.

Keywords: Thermal cycling; energy release rate; shear-lag analysis; modified Paris law.

1. INTRODUCTION

Carbon Fiber Reinforced Plastics (CFRP) are used in the form of multidirectional laminates. Thermal stress in the plies is induced as a result of the temperature change from the cure temperature, due to a large difference of thermal expansion coefficients of the plies [1, 2]. If the temperature changes periodically, the thermal stresses also change periodically. Periodic thermal stresses often cause matrix cracking in laminates, which degrade mechanical properties of the laminates [1–5]. If the application of CFRP to a space structure is considered, it is important to understand the matrix cracking behavior induced by periodic thermal stresses due to the solar eclipse, etc.

*To whom all correspondence should addressed.

In the present study, microscopic damage such as matrix cracking was observed in high temperature CFRP AS4/PEEK cross-ply laminates under thermal cycling condition. Damage progress was analyzed using shear-lag analysis [3, 4].

2. EXPERIMENTAL PROCEDURE

Thermal cycling tests were conducted for carbon fiber reinforced polyetheretherketone (AS4/PEEK). Polyetheretherketone (PEEK) is thermoplastic resin that has a well defined glass transition temperature (143°C) with corresponding significant changes in coefficient of thermal expansion and elastic properties [6]. The mechanical properties of AS4/PEEK are showed in Table 1. The stress-free temperature of the laminate is 310°C. In the experiment, two kinds of cross-ply laminates, $[0_2/90_3/0_2]$ and $[0_2/90_4/0_2]$, were used. In the present study, the outer ply was defined as the 0° ply. Figure 1 shows the geometry of the specimen for thermal cycling test. All edge surfaces of the specimens were polished for damage observation. Before testing, all specimens were dried in a vacuum chamber to eliminate the moisture effects. In-house thermal cycle test equipment that consisted of a liquid nitrogen (LN_2) vessel and ceramic fiber heaters was developed. First, specimens

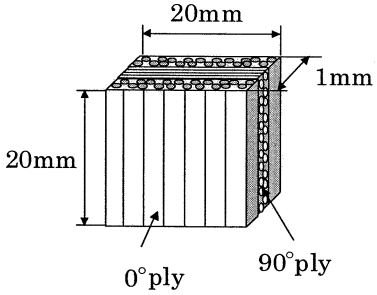

Figure 1. Specimen geometry for thermal cycling test.

Table 1.
Mechanical properties of AS4/PEEK at various temperatures

	Temperature [°C]					
	0	50	100	150	200	250
Longitudinal tensile modulus E_1 [GPa]	134	134	134	134	134	134
Transverse tensile modulus E_2 [GPa]	10.0	8.9	7.9	5.6	3.2	1.5
In-plane Poisson's ratio ν_{12}	0.31	0.31	0.31	0.5	0.5	0.5
Longitudinal thermal expansion coefficient α_1 [$\mu\varepsilon/K$]	0.6	0.6	0.6	0.6	0.6	0.6
Transverse thermal expansion coefficient α_2 [$\mu\varepsilon/K$]	29.1	29.1	29.1	80.0	80.0	80.0
*Out-of-plane Poisson's ratio ν_{23}	0.5	0.5	0.5	0.5	0.5	0.5

* Assumed value.

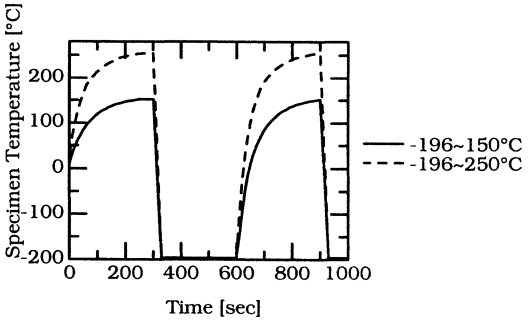

Figure 2. Specimen temperature as a function of time.

were heated up to 150°C or 250°C by ceramic fiber heaters. Then, they were cooled down to −196°C, that is, the boiling point of LN_2. Specimens were held in each environment for 5 min. Figure 2 shows the specimen temperature as a function of time. The thermal cycling test in −196 to 150°C range was conducted up to 1000 cycles, and that in −196 to 250°C range was conducted up to 500 cycles. The microscopic damage was observed with an optical microscope and soft X-ray radiography. The matrix crack density was defined as the number of matrix cracks per unit observed length.

3. EXPERIMENTAL RESULTS

3.1. Matrix crack progress

With the optical microscope, matrix cracks induced by cyclic thermal stress were observed in both 0° and 90° plies. Figures 3 and 4 show the edge views of matrix crack in 0° and 90° plies, respectively. With these observations, matrix cracks were found to extend to the full thickness of 0° and 90° plies. Figure 5 shows a sequence of soft X-ray radiography observations (−196 to 250°C temperature range, $[0_2/90_4/0_2]$). With the soft X-ray radiography, matrix cracks were found to extend to the full width and height of 0° and 90° plies. Soft X-ray radiography indicated that crack initiation occurred not only from the specimen edge but also from the crack tips in 0° plies. Figure 6 shows the schematic of matrix crack progress in 90° plies. The high stress intensity near the tip of matrix cracks in 0° plies tends to generate the matrix crack initiation in 90° plies.

Figures 7 to 10 show the crack density in each ply as a function of the number of thermal cycles. For the thermal cycling in −196 to 150°C range, at the early stage of this thermal cycling, the number of matrix cracks in 0° plies grew more rapidly than that in 90° plies. After a few hundred cycles, the matrix crack density growth rate of 90° plies became larger than that of 0° plies. Eventually the matrix crack density of 90° plies became larger than that of 0° plies.

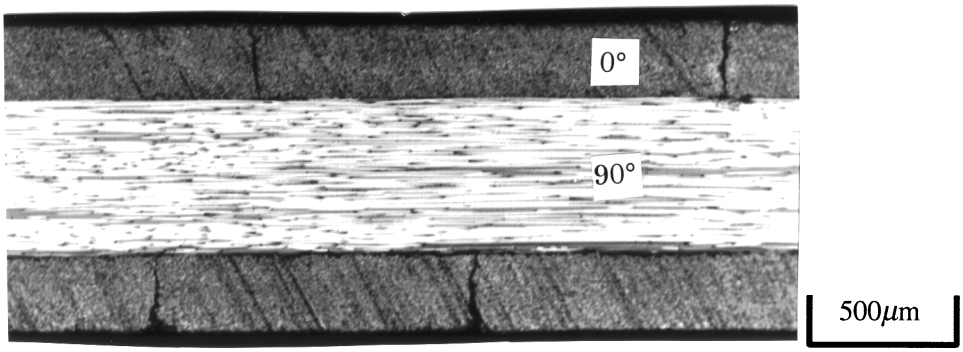

Figure 3. Matrix crack in 0° plies (−196 to 250°C, $[0_2/90_4/0_2]$, 200 cycles).

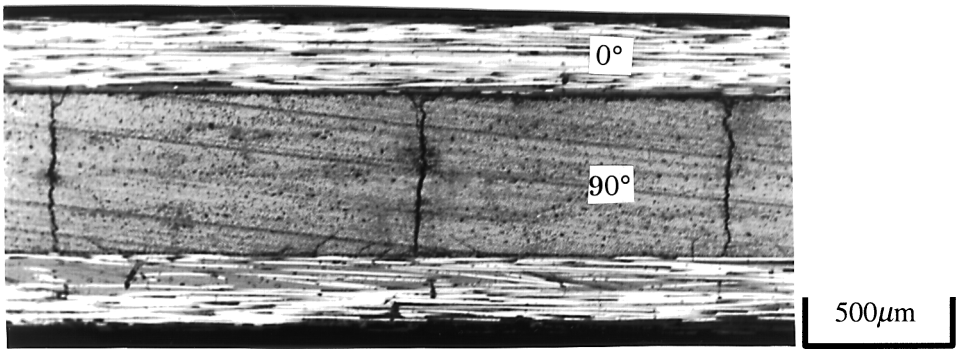

Figure 4. Matrix crack in 90° plies (−196 to 250°C, $[0_2/90_4/0_2]$, 200 cycles).

For the thermal cycling in −196 to 250°C range, matrix cracks in both 0° and 90° plies initiate simultaneously. The matrix crack density seemed to reach the saturation level approximately at 500 cycles.

There was a tendency that the matrix crack density saturation level of 90° plies was approximately twice as large as that of 0° plies. In $[0_2/90_3/0_2]$ laminate, the matrix crack growth rate of 90° plies was larger than that in $[0_2/90_4/0_2]$ laminate.

3.2. Delamination progress

For the thermal cycling in −196 to 150°C range, no other damage, such as delamination or fiber fractures, except matrix cracks, was observed before 1000 thermal cycles. On the other hand, for the thermal cycling in −196 to 250°C range, delaminations which evolved along matrix cracks in 0° plies were observed approximately after 200 thermal cycles, as shown in Fig. 5. After 500 cycles, the delaminations could be seen as black-regions, which spread along matrix cracks in 0° plies. Figure 11 shows the delamination initiating from the tip of a matrix crack in 0° plies.

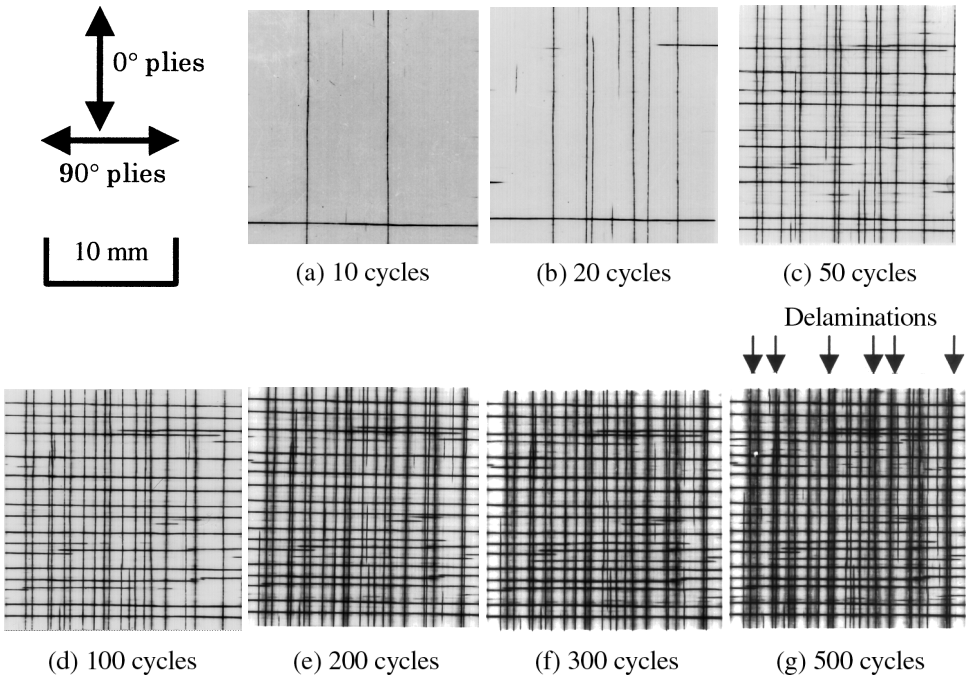

Figure 5. Soft X-ray radiography observation. Temperature range was −196 to 250 °C. Laminate configuration was $[0_2/90_4/0_2]$.

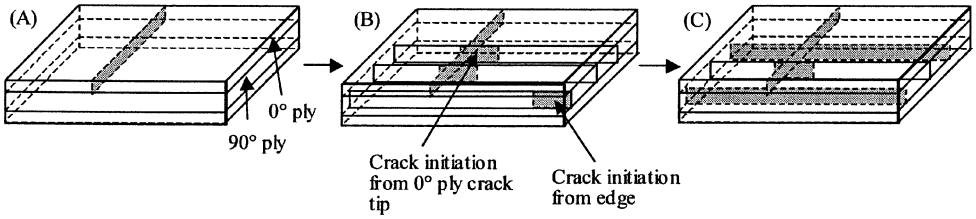

Figure 6. Schematic of matrix crack progress in 90° plies.

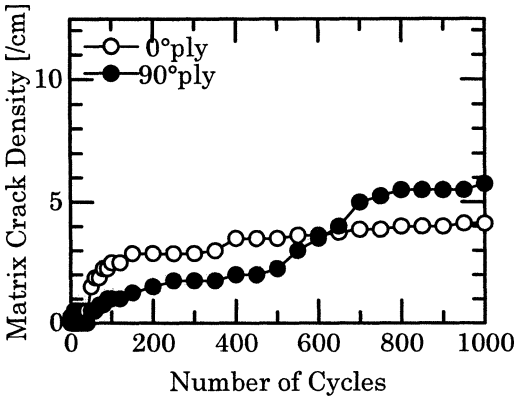

Figure 7. Matrix crack density as a function of thermal cycle number [−196 to 150 °C], $[0_2/90_3/0_2]$.

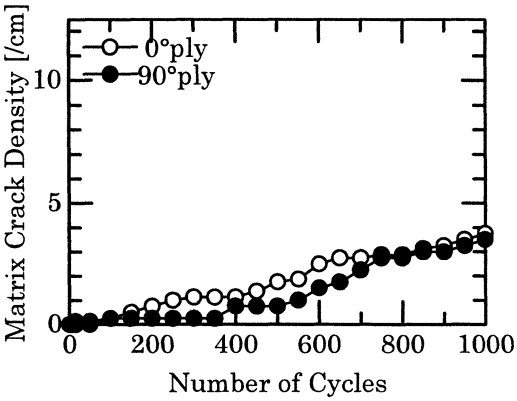

Figure 8. Matrix crack density as a function of thermal cycle number [−196 to 150 °C], $[0_2/90_4/0_2]$.

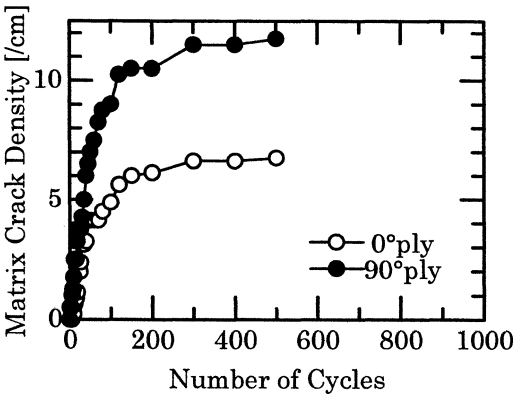

Figure 9. Matrix crack density as a function of thermal cycle number [−196 to 250 °C], $[0_2/90_3/0_2]$.

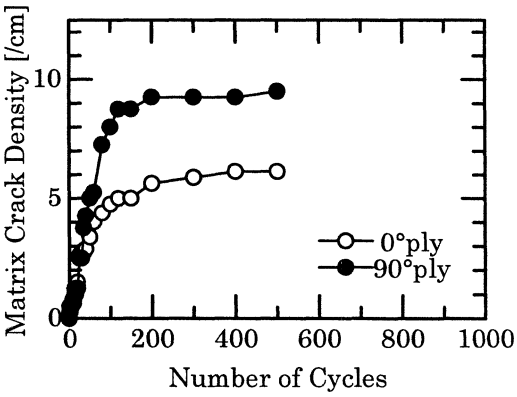

Figure 10. Matrix crack density as a function of thermal cycle number [−196 to 250 °C], $[0_2/90_4/0_2]$.

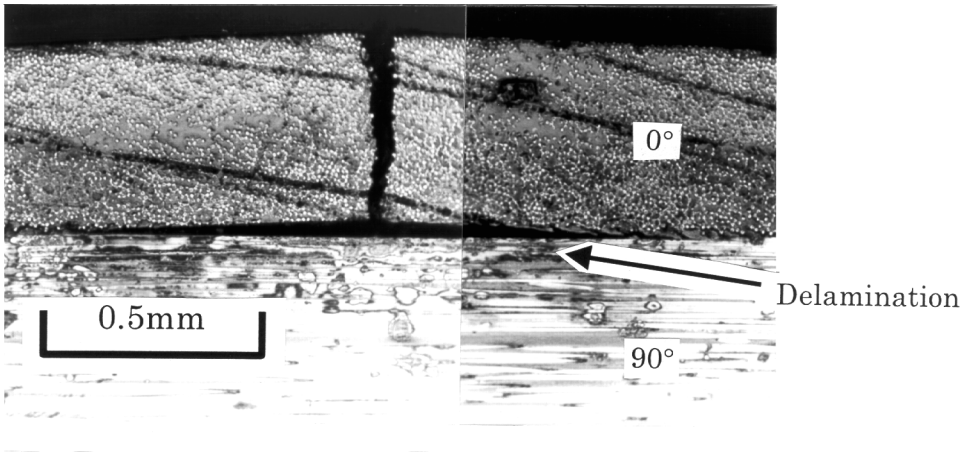

Figure 11. Delamination from the tip of matrix crack in 0° plies.

4. DISCUSSION

In order to explain these experimental results, the stress field of a cross-ply laminate which contains cracks in both 0° and 90° plies was calculated by using the shear-lag analysis [3, 4]. Energy release rate associated with matrix cracking was calculated as follows.

$$G = -\frac{\partial\left[t_0\left(\overline{\sigma_x^0}\left(\frac{\overline{\sigma_x^0}}{E_1^{0c}} - \frac{\nu_{12}^{0c}\overline{\sigma_y^0}}{E_1^{0c}}\right) + \left(\overline{\sigma_y^0}\left(\frac{\overline{\sigma_y^0}}{E_2^{0c}} - \frac{\nu_{12}^{0c}\overline{\sigma_x^0}}{E_1^{0c}}\right)\right)\right)\right]}{2\partial(t_0 d_0 + t_{90} d_{90})}$$
$$-\frac{\partial\left[t_{90}\left(\overline{\sigma_x^{90}}\left(\frac{\overline{\sigma_x^{90}}}{E_2^{90c}} - \frac{\nu_{12}^{90c}\overline{\sigma_y^{90}}}{E_1^{90c}}\right) + \left(\overline{\sigma_y^{90}}\left(\frac{\overline{\sigma_y^{90}}}{E_1^{90c}} - \frac{\nu_{12}^{90c}\overline{\sigma_x^{90}}}{E_1^{90c}}\right)\right)\right)\right]}{2\partial(t_0 d_0 + t_{90} d_{90})}, \quad (1)$$

where t_θ is half thickness of θ° plies, d_θ is matrix crack density in θ° plies, $\overline{\sigma_i^\theta}$ is average stress in i direction in θ° plies. $E_1^{\theta c}$, $E_2^{\theta c}$, $\nu_{12}^{\theta c}$ (Young's modulus along the fibers, Young's modulus transverse to the fibers and major Poisson's ratio, respectively) are the elastic constants of the cracked θ° plies calculated using shear-lag analysis, as shown in the Appendix. The energy release rate range ΔG was calculated using equation (1).

In order to relate ΔG to the matrix crack density, the modified Paris law [5] was used. The conventional Paris law approach relates the crack growth rate to the range in the applied stress intensity factor. Nairn and his coworkers proposed analysing fatigue data using a modified Paris law approach [5]. In their analysis, the energy release rate range was used instead of the range in stress intensity factor, and the transverse crack density was substituted instead of the crack length. In the modified

Paris law analysis, the matrix crack density growth rate is given by

$$\frac{\mathrm{d}D}{\mathrm{d}N} = A\Delta G^n, \tag{2}$$

where A and n are two power-law fitting parameters, D is matrix crack density and N is the number of thermal cycling. If equation (2) is valid, plotting $\mathrm{d}D/\mathrm{d}N$ as a function of ΔG on a log–log scale should yield a linear relation. Furthermore, in the present study, another power-law relation was assumed between the stress amplitude in cracked plies ($\Delta\sigma_{\max}$) and $\mathrm{d}D/\mathrm{d}N$ as follows.

$$\frac{\mathrm{d}D}{\mathrm{d}N} = B(\Delta\sigma_{\max})^m, \tag{3}$$

where B and m are two power-law fitting parameters.

The experimental results could be rearranged from the following three points of view.

Point 1. The difference in temperature range of thermal cycling (−196 to 150°C or −196 to 250°C).

Point 2. The difference in ply thickness ($[0_2/90_3/0_2]$ or $[0_2/90_4/0_2]$).

Point 3. The difference in position of cracked layer (inner or outer).

As regards Point 1, there is a positive correlation between ΔG and $\mathrm{d}D/\mathrm{d}N$, because ΔG in −196 to 250°C range is larger than that in −196 to 150°C. Moreover, there is also positive correlation between $\Delta\sigma_{\max}$ and $\mathrm{d}D/\mathrm{d}N$, because $\Delta\sigma_{\max}$ in −196 to 250°C range is larger than that in −196 to 150°C. For example, the matrix crack density growth rate in Fig. 9 is much larger than that in Fig. 7. These experimental results are consistent with equations (2) and (3).

As regards Point 2, there is a negative correlation between ΔG and $\mathrm{d}D/\mathrm{d}N$, because the thicker the cracked plies, the larger is ΔG. Figures 12 and 13 show

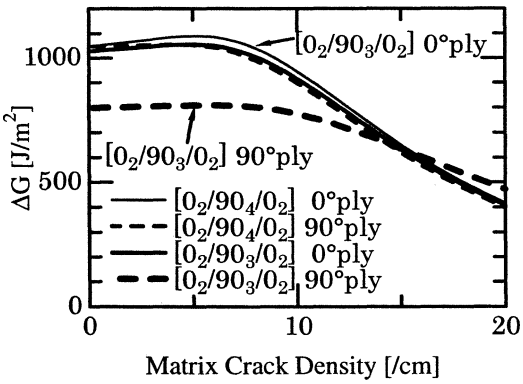

Figure 12. Energy release rate range as a function of matrix crack density. Thermal cycle range was −196 to 250°C.

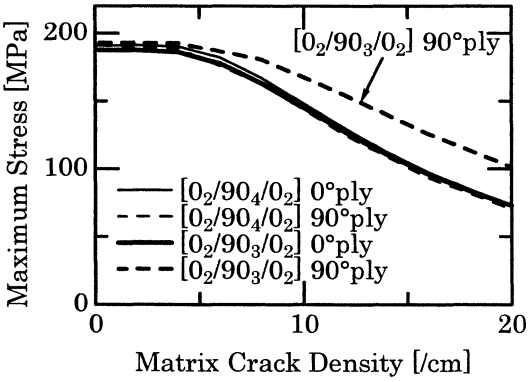

Figure 13. Maximum stress at −196 °C as a function of matrix crack density.

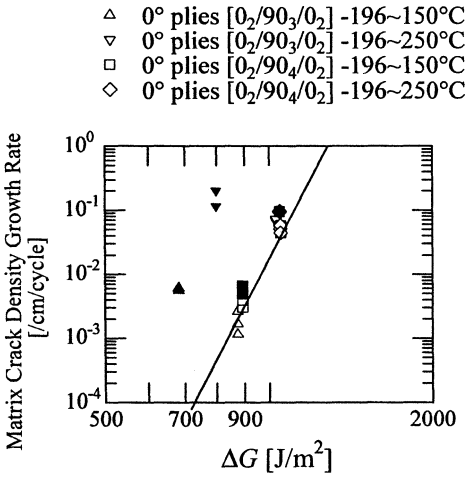

Figure 14. Matrix crack density growth rate as a function of ΔG.

analytical results of the energy release rate range and the maximum stress as a function of matrix crack density. In Fig. 12, $\mathrm{d}D/\mathrm{d}N$ of 90° plies in $[0_2/90_3/0_2]$ laminate is larger than that in $[0_2/90_4/0_2]$ laminate. This result is inconsistent with equation (2). However, there is a positive correlation between $\sigma_{\max}$ and $\mathrm{d}D/\mathrm{d}N$, because the thicker the clacked plies are, the smaller $\sigma_{\max}$ is. In Fig. 13, the maximum stress of the $[0_2/90_3/0_2]$ 90° ply, keeps a higher level than others. This analytical result is consistent with the experimental result. This result is also consistent with equation (3).

As regards Point 3, in the shear-lag analysis [3, 4], the ply modulus variation is dependent only on the ply thickness and the crack density. Then the energy release rate associated with matrix cracking in 0° plies is equal to that in 90° plies, when $t_0 = t_{90}$ and $d_0 = d_{90}$. Therefore, this analytical result indicates that in $[0_2/90_4/0_2]$

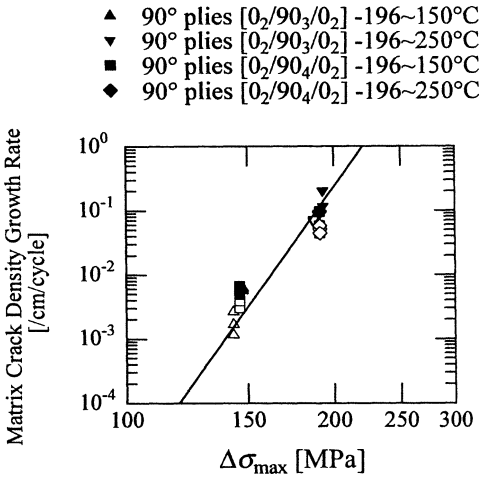

Figure 15. Matrix crack density growth rate as a function of $\Delta\sigma_{\max}$.

laminate ΔG associated with matrix cracking in 0° plies is equal to ΔG associated with matrix cracking in 90° plies. However, Fig. 10 indicates that both the saturation level and the growth rate of crack density in 90° ply is twice as large as that in 0° plies. This experimental result is inconsistent with the above-mentioned analytical result. Thus, in order to consider matrix cracks in the outer plies, we must use other analytical models, which should be modified on the assumption of different displacement fields.

From these analyses and experimental data, $\mathrm{d}D/\mathrm{d}N$ was plotted as a function of ΔG or $\Delta\sigma_{\max}$ on a log–log plot. Figures 14 and 15 show $\mathrm{d}D/\mathrm{d}N$ as a function of ΔG and $\Delta\sigma_{\max}$, respectively. Data in Fig. 15 seem to fall on a master curve. On the other hand, data in Fig. 14 have less correlation than that in Fig. 15. This means that, in this study, $\mathrm{d}D/\mathrm{d}N - \Delta\sigma_{\max}$ analysis is better than the modified Paris law analysis for the present laminate configuration.

5. CONCLUSIONS

Thermal cycling tests were conducted for two types of AS4/PEEK cross-ply laminates. Matrix cracks were observed in both 0° and 90° plies of both laminates. To explain the matrix crack progress, shear-lag analysis was used to calculated the ply stress and energy release rate associated with matrix cracking. Comparing the maximum stress amplitude analysis with the energy release rate range analysis, the maximum stress amplitude analysis provided a better explanation of the experimental results for the present laminate configuration. Further analysis is necessary to generalize the present conclusion.

REFERENCES

1. G. P. Fang, R. A. Schapery and Y. Weitsman, Thermally-induced fracture in composites, *Engineering Fracture Mechanics* **33** (4), 619–632 (1989).
2. Hugh L. McManus, Prediction of thermal cycling induced matrix cracking, *J. Reinf. Plast. Compos.* **15**, 124–140 (1996).
3. C. Henaff-Gardin, M. C. Lafarie-Frenot and D. Gamby, Doubly periodic matrix cracking in composite laminates, Part 1: General in-plane loading, *Compos. Struct.* **36**, 113–130 (1996).
4. C. Henaff-Gardin, M. C. Lafarie-Frenot and D. Gamby, Doubly periodic matrix cracking in composite laminates, Part 2: Thermal biaxial loading, *Compos. Struct.* **36**, 131–140 (1996).
5. John A. Nairn, Microracking, microcrack-induced delamination, and longitudinal splitting of advanced composite structures, *NASA Contractor Report* **4472** (1992).
6. G. Jeronimidis and A. T. Parkyn, Residual stresses in carbon fibre-thermoplastic matrix laminates, *J. Compos. Mater.* **22**, 401–415 (1988).

APPENDIX

The parameters $(\overline{\sigma_i^{\theta}}, E_1^{\theta c}, E_2^{\theta c}, \nu_{12}^{\theta c})$ in equation (1) are shown as follows.

$$\overline{\sigma_x^0} = -\frac{t_{90}}{t_0}\overline{\sigma_x^{90}} = A'\frac{2d_{90}}{R\lambda_x}\sinh\left(\frac{R\lambda_x}{2d_{90}}\right) + B'\frac{2d_0}{R\lambda_y}\sinh\left(\frac{R\lambda_y}{2d_0}\right) + K'_x,$$

$$\overline{\sigma_y^0} = -\frac{t_{90}}{t_0}\overline{\sigma_y^{90}} = A'\frac{\nu_{12}E_2(t_0+t_{90})}{t_0E_2+t_{90}E_1}\frac{2d_{90}}{R\lambda_x}\sinh\left(\frac{R\lambda_x}{2d_{90}}\right) + B'\frac{t_{90}E_2+t_0E_1}{\nu_{12}E_2(t_0+t_{90})}\frac{2d_0}{R\lambda_y}\sinh\left(\frac{R\lambda_y}{2d_0}\right) + K'_y,$$

$$E_1^{90c} = \frac{f_{4x}f_{3y} - f_{3x}f_{4y}}{\left(-\frac{\nu_{12}}{E_1}f_{1x} + \frac{1}{E_2}f_{2x}\right)f_{3y} - \left(-\frac{\nu_{12}}{E_1}f_{1y} + \frac{1}{E_2}f_{2y}\right)f_{3x}},$$

$$E_2^{90c} = \frac{f_{4x}f_{3y} - f_{3x}f_{4y}}{\left(\frac{\nu_{12}}{E_1}f_{2x} - \frac{1}{E_1}f_{1x}\right)f_{4y} - \left(\frac{\nu_{12}}{E_1}f_{2y} - \frac{1}{E_1}f_{1y}\right)f_{4x}},$$

$$\nu_{12}^{90c} = \frac{E_1^{90c}}{f_{4x}}\left(\frac{1}{E_2^{90c}}f_{3x} - \frac{1}{E_1}f_{1x} + \frac{\nu_{12}}{E_1}f_{2x}\right),$$

$$\nu_{21}^{90c} = \frac{E_2^{90c}}{f_{3x}}\left(\frac{1}{E_1^{90c}}f_{4x} - \frac{1}{E_2}f_{2x} + \frac{\nu_{12}}{E_1}f_{1x}\right),$$

$$E_1^{0c} = \frac{g_{1x}g_{2y} - g_{2x}g_{1y}}{\left(\frac{1}{E_2}g_{3x} - \frac{\nu_{12}}{E_1}g_{4x}\right)g_{2y} - \left(\frac{1}{E_2}g_{3y} - \frac{\nu_{12}}{E_1}g_{4y}\right)g_{2x}},$$

$$E_2^{0c} = \frac{g_{2x}g_{1y} - g_{1x}g_{2y}}{\left(-\frac{\nu_{12}}{E_1}g_{3x} + \frac{1}{E_1}g_{4x}\right)g_{1y} - \left(-\frac{\nu_{12}}{E_1}g_{3y} + \frac{1}{E_1}g_{4y}\right)g_{1x}},$$

$$\nu_{12}^{0c} = \frac{E_1^{0c}}{g_{2x}}\left(\frac{1}{E_1^{0c}}g_{1x} - \frac{1}{E_2}g_{3x} + \frac{\nu_{12}}{E_1}g_{4x}\right),$$

$$\nu_{21}^{0c} = \frac{E_2^{0c}}{g_{1x}}\left(\frac{1}{E_2^{0c}}g_{2x} - \frac{1}{E_1}g_{4x} + \frac{\nu_{12}}{E_1}g_{3x}\right),$$

$$f_{1x}(d_{90}) = \left(\frac{t_0+t_{90}}{t_0} - K_{xx}\right)\frac{2d_{90}}{R\lambda_x}\tanh\left(\frac{R\lambda_x}{2d_{90}}\right) + K_{xx},$$

$$f_{2x}(d_{90}) = \left(\frac{t_0+t_{90}}{t_0} - K_{xx}\right)\frac{\nu_{12}E_2(t_0+t_{90})}{t_0E_2+t_{90}E_1}\frac{2d_{90}}{R\lambda_x}\tanh\left(\frac{R\lambda_x}{2d_{90}}\right) + K_{yx},$$

$$f_{3x}(d_{90}) = -\left(\frac{t_0+t_{90}}{t_0} - K_{xx}\right)\frac{t_0}{t_{90}}\frac{2d_{90}}{R\lambda_x}\tanh\left(\frac{R\lambda_x}{2d_{90}}\right) + \frac{t_0+t_{90}}{t_{90}} - K_{xx}\frac{t_0}{t_{90}},$$

$$f_{4x}(d_{90}) = -\left(\frac{t_0+t_{90}}{t_0} - K_{xx}\right)\frac{t_0}{t_{90}}\frac{\nu_{12}E_2(t_0+t_{90})}{t_0E_2+t_{90}E_1}\frac{2d_{90}}{R\lambda_x}\tanh\left(\frac{R\lambda_x}{2d_{90}}\right) - K_{yx}\frac{t_0}{t_{90}},$$

$$f_{1y}(d_{90}) = -K_{xy}\frac{2d_{90}}{R\lambda_x}\tanh\left(\frac{R\lambda_x}{2d_{90}}\right) + K_{xy},$$

$$f_{2y}(d_{90}) = -K_{xy}\frac{\nu_{12}E_2(t_0+t_{90})}{t_0E_2+t_{90}E_1}\frac{2d_{90}}{R\lambda_x}\tanh\left(\frac{R\lambda_x}{2d_{90}}\right) + K_{yy},$$

$$f_{3y}(d_{90}) = K_{xy}\frac{t_0}{t_{90}}\frac{2d_{90}}{R\lambda_x}\tanh\left(\frac{R\lambda_x}{2d_{90}}\right) - K_{xy}\frac{t_0}{t_{90}},$$

$$f_{4y}(d_{90}) = K_{xy}\frac{t_0}{t_{90}}\frac{\nu_{12}E_2(t_0+t_{90})}{t_0E_2+t_{90}E_1}\frac{2d_{90}}{R\lambda_x}\tanh\left(\frac{R\lambda_x}{2d_{90}}\right) - K_{yy}\frac{t_0}{t_{90}} + \frac{t_0+t_{90}}{t_{90}},$$

$$g_{1x}(d_0) = -K_{yx}\frac{\nu_{12}E_2(t_0+t_{90})}{t_0E_1+t_{90}E_2}\frac{2d_0}{R\lambda_y}\tanh\left(\frac{R\lambda_y}{2d_0}\right) + K_{xx},$$

$$g_{2x}(d_0) = -K_{yx}\frac{2d_0}{R\lambda_y}\tanh\left(\frac{R\lambda_y}{2d_0}\right) + K_{yx},$$

$$g_{3x}(d_0) = K_{yx}\frac{\nu_{12}E_2(t_0+t_{90})}{t_0E_1+t_{90}E_2}\frac{t_0}{t_{90}}\frac{2d_0}{R\lambda_y}\tanh\left(\frac{R\lambda_y}{2d_0}\right) + \frac{t_0+t_{90}}{t_{90}} - K_{xx}\frac{t_0}{t_{90}},$$

$$g_{4x}(d_0) = K_{yx}\frac{t_0}{t_{90}}\left(\frac{2d_0}{R\lambda_y}\tanh\left(\frac{R\lambda_y}{2d_0}\right) - 1\right),$$

$$g_{1y}(d_0) = -K_{yy}\frac{\nu_{12}E_2(t_0+t_{90})}{t_0E_1+t_{90}E_2}\frac{2d_0}{R\lambda_y}\tanh\left(\frac{R\lambda_y}{2d_0}\right) + K_{xy},$$

$$g_{2y}(d_0) = -K_{yy}\frac{2d_0}{R\lambda_y}\tanh\left(\frac{R\lambda_y}{2d_0}\right) + K_{yy},$$

$$g_{3y}(d_0) = K_{yy}\frac{t_0}{t_{90}}\frac{\nu_{12}E_2(t_0+t_{90})}{t_0E_1+t_{90}E_2}\frac{2d_0}{R\lambda_y}\tanh\left(\frac{R\lambda_y}{2d_0}\right) - K_{xy}\frac{t_0}{t_{90}},$$

$$g_{4y}(d_0) = K_{yy}\frac{t_0}{t_{90}}\left(\frac{2d_0}{R\lambda_y}\tanh\left(\frac{R\lambda_y}{2d_0}\right)-1\right) + \frac{t_0+t_{90}}{t_{90}},$$

$$K_{xx} = \frac{\mu_x^2\mu_y^2}{\mu_x^2\mu_y^2-\lambda_x^2\lambda_y^2}\left(1-\frac{\lambda_y^2}{\mu_y^2}\frac{E_1}{\nu_{12}E_2}\right),$$

$$K_{xy} = \frac{\mu_x^2\mu_y^2}{\mu_x^2\mu_y^2-\lambda_x^2\lambda_y^2}\left(\frac{\lambda_y^2}{\mu_y^2}-\frac{1}{\nu_{12}}\right),$$

$$K_{yx} = \frac{\mu_x^2\mu_y^2}{\mu_x^2\mu_y^2-\lambda_x^2\lambda_y^2}\left(\frac{\lambda_x^2}{\mu_x^2}-\frac{E_1}{\nu_{12}E_2}\right),$$

$$K_{yy} = \frac{\mu_x^2\mu_y^2}{\mu_x^2\mu_y^2-\lambda_x^2\lambda_y^2}\left(1-\frac{\lambda_x^2}{\mu_x^2}-\frac{1}{\nu_{12}}\right),$$

$$R = \sqrt{1-\frac{\mu_x^2\mu_y^2}{\lambda_x^2\lambda_y^2}},$$

$$A' = \frac{K_x'\frac{(t_0E_1+t_{90}E_2)}{\nu_{12}E_2(t_0+t_{90})}\cosh\left(\frac{R\lambda_y}{2d_0}\right) - K_y'\frac{2d_0}{R\lambda_y}\sinh\left(\frac{R\lambda_y}{2d_0}\right)}{\frac{2d_{90}}{R\lambda_x}\frac{2d_0}{R\lambda_y}\frac{\nu_{12}E_2(t_0+t_{90})}{t_0E_2+t_{90}E_1}\sinh\left(\frac{R\lambda_x}{2d_{90}}\right)\sinh\left(\frac{R\lambda_y}{2d_0}\right) - \frac{(t_0E_1+t_{90}E_2)}{\nu_{12}E_2(t_0+t_{90})}\cosh\left(\frac{R\lambda_x}{2d_{90}}\right)\cosh\left(\frac{R\lambda_y}{2d_0}\right)},$$

$$B' = \frac{-K_x'\frac{\nu_{12}E_2(t_0+t_{90})}{(t_0E_2+t_{90}E_1)}\frac{2d_{90}}{R\lambda_x}\sinh\left(\frac{R\lambda_x}{2d_{90}}\right) + K_y'\cosh\left(\frac{R\lambda_x}{2d_{90}}\right)}{\frac{2d_{90}}{R\lambda_x}\frac{2d_0}{R\lambda_y}\frac{\nu_{12}E_2(t_0+t_{90})}{t_0E_2+t_{90}E_1}\sinh\left(\frac{R\lambda_x}{2d_{90}}\right)\sinh\left(\frac{R\lambda_y}{2d_0}\right) - \frac{(t_0E_1+t_{90}E_2)}{\nu_{12}E_2(t_0+t_{90})}\cosh\left(\frac{R\lambda_x}{2d_{90}}\right)\cosh\left(\frac{R\lambda_y}{2d_0}\right)},$$

$$K_x' = \frac{\xi_x\lambda_y^2-\xi_y\mu_x^2}{\mu_x^2\mu_y^2-\lambda_x^2\lambda_y^2}\Delta T,$$

$$K_y' = \frac{\xi_x\mu_y^2-\xi_y\lambda_x^2}{\mu_x^2\mu_y^2-\lambda_x^2\lambda_y^2}\Delta T,$$

$$\lambda_x^2 = \frac{3G_{23}}{t_0t_{90}{}^2}\frac{(t_0E_1+t_{90}E_2)}{E_1E_2},$$

$$\lambda_y^2 = \frac{3G_{23}}{t_0{}^2t_{90}}\frac{(t_{90}E_1+t_0E_2)}{E_1E_2},$$

$$\mu_x^2 = \frac{3G_{23}}{t_0t_{90}{}^2}(t_0+t_{90})\frac{\nu_{12}}{E_1},$$

$$\mu_y^2 = \frac{3G_{23}}{t_0{}^2t_{90}}(t_0+t_{90})\frac{\nu_{12}}{E_1},$$

$$\xi_x = \frac{3G_{23}}{t_0 t_{90}}(\alpha_1 - \alpha_2),$$

$$\xi_y = \frac{3G_{23}}{t_0^2}(\alpha_1 - \alpha_2),$$

$$\Delta T = T - T_{\mathrm{sf}},$$

where T_{sf} is the stress-free temperature.